International Journal of Nanomedicine

Dovepress
open access to scientific and medical research

Open Access Full Text Article

ORIGINAL RESEARCH

Fabrication of a Novel Au Star@AgAu Yolk-Shell Nanostructure for Ovarian Cancer Early Diagnosis and Targeted Therapy

Ting Lan[1,*], Yang Zhao[1,2,*], Yu Du[1,3,*], Chunyi Ma[1], Rui Wang[1], Qianlei Zhang[1], Shanshan Wang[1], Wenxian Wei[4], Honghua Yuan[2], Qingli Huang[1,2]

[1]Medical Technology School of Xuzhou Medical University, Xuzhou City, Jiangsu, 221000, People's Republic of China; [2]Public Experimental Research Center of Xuzhou Medical University, Xuzhou City, Jiangsu, 221004, People's Republic of China; [3]Xuzhou Center for Disease Control and Prevention, Xuzhou City, Jiangsu, 221006, People's Republic of China; [4]Testing Center, Yangzhou University, Yangzhou City, Jiangsu, 225009, People's Republic of China

*These authors contributed equally to this work

Correspondence: Honghua Yuan, Public Experimental Research Center of Xuzhou Medical University, Tong Shan No. 209, Xuzhou, 221004, People's Republic of China, Tel/Fax +86-516-83262091, Email XUYIyhh@xzhmu.edu.cn; Qingli Huang, Medical Technology School, Public Experimental Research Center of Xuzhou Medical University, Tong Shan No. 209, Xuzhou, 221004, People's Republic of China, Tel/Fax +86-516-83262091, Email qlhuang@xzhmu.edu.cn

Purpose: A novel CYPA-targeted, SiO_2 encapsulated Au star@AgAu yolk-shell nanostructure (YSNS) was synthesized and used for ovarian cancer early diagnosis and therapy.

Methods: Diverse spectroscopic and microscopic methods were utilized to investigate the pattern of the yolk-shell nanostructure. In addition, in vitro and in vivo experiments were carried out.

Results: It can be found that the ratio of $HAuCl_4$ and $AgNO_3$ played a critical role in the constitution of the yolk-shell nanostructure. The as-prepared yolk-shell nanostructure showed excellent SERS performance, which could be utilized as SERS substrate for specific sensitivity analysis of ovarian cancer markers cyclophilin A (CYPA) with detectable limit of $7.76*10^{-10}$ μg/mL. In addition, the as-prepared yolk-shell nanostructure possessed outstanding photothermal performance, which could be used as photothermal agent for ovarian cancer therapy. Experiments in vitro and in vivo proved that the as-prepared yolk-shell nanostructures are ideal candidate for early diagnosis and therapy for ovarian cancer in one platform.

Conclusion: This work holds promise to offer a new method for the detection and therapy of ovarian cancer in the early stage.

Keywords: yolk-shell nanostructure, surface-enhanced Raman scattering, early diagnosis, cancer targeted therapy

Introduction

There are numerous genital tumors that threaten women's health around the world, one among them is ovarian cancer. In 2022, the American Cancer Society estimates that an additional 19,880 women will suffer from ovarian cancer and 12,810 deaths.[1] In the early stage, the clinical symptoms of ovarian cancer are relatively hidden and difficult to be detected, so most patients cannot be diagnosed until the advanced stage, missing the best treatment opportunity.[2,3] Therefore, it is urgent to explore the effective biomarkers and methods for diagnosis of the early stage of ovarian cancer. Currently, there are only a few publicly recognized ovarian cancer tumor markers, carbohydrate antigen 125 (CA125) and humanepididymisprotein4 (HE4) which were most used in clinical.[4–7] However, when the stage of benign ovarian cyst, hysteromyoma, infection, the sensitivity and specificity are poorer, the overall showed a trend of increase [8]. According to previous reports and our research, the concentration of CYPA in patients with early ovarian cancer was significantly increased, compared with healthy women and benign group, and the proportion of CYPA positive reaction was higher in I/II stage.[8–10] In addition, the secretion of CYPA in serous ovarian cancer is much higher than that in nearby tissues, and

Received: 21 March 2023
Accepted: 22 June 2023
Published: 10 July 2023

Graphical Abstract

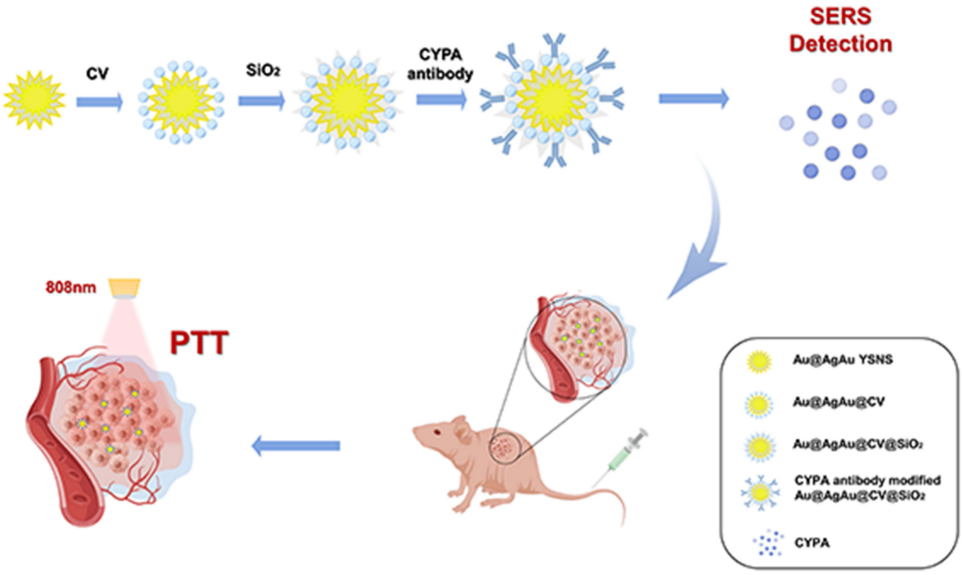

the advanced of ovarian cancer is also closely related to the expression of CYPA.[10] All these indicate that the overexpression of CYPA is intimately associated with the occurrence of ovarian cancer. At present, most of the detection methods of CYPA are chemiluminescence and ELISA, but their detection limit is about 10^{-4}–10^{-5}μg/mL, which makes its clinical application in early diagnosis of tumors greatly limited.[4,11–14]

Surface-enhanced Raman spectroscopy (SERS) is an ideal approach to solving problems above attributed to its high sensitivity, straightforward, and simple, which has been extensively studied and applied in medical diagnosis, chemistry, biology, environment and other fields.[15–19] For SERS application, SERS active nanomaterials are essential.[20–23] Precious metals represented by gold and silver are relatively popular and have great development potential. Ag nanostructures have been widely favored in the application of SERS. However, its chemical properties are not very stable and its surface is easy to be oxidized, which has become the most difficult drawback for Ag to become SERS substrate. On the contrary, nanostructured Au has a lower damping rate, a more stable structure and greater biocompatibility, but its ability to enhance SERS is much lower than that of Ag nanoparticles of the same size. These characteristics greatly restricted the application of SERS employing single metal Au and Ag nanomaterials. Comparatively, bimetallic nanoparticles have attracted attention for their good chemical stability, enhanced catalytic and SERS properties.[15,24–28] Some Au-Ag nano-alloys or Au@Ag nano-hybrids with enhanced catalytic or SERS properties were also prepared in the past decades.[23–27] However, we still require to focus on the unique shape, size and internal hierarchy of bimetallic nano hybrid materials, and constantly design and attempt to obtain better SERS performance.

In addition to early diagnosis, conventional tumor treatment has some limitations, which makes the early therapy of tumor become a difficult problem in the present. For example, surgery is invasive treatment and cannot accurately remove the nidus that are invisible in the stage of cancer. Radiotherapy and chemotherapy can cause many adverse effects, which will damage to normal tissue. Recently, photothermal therapy (PTT), due to its special advantages in improving the specificity of tumor detection and reducing the side effects of tumor treatment, it has attracted wide attention.[29–31] The basic principle of photothermal therapy is that nanomaterials with light conversion function (photothermal nanoagents) accumulated at the tumor site and elevated the local temperature by absorbing the energy of light and converting light energy into heat energy. When the local temperature reaches 42−47°C, the tumor cells can be quickly killed and cleared.[32–34] Compared to other photothermal agents, gold nanomaterials are considered as promising anti-tumor photothermal therapy agents. They can form a transient excited state in light, and they can also efficiently

convert light energy into internal energy. Owing to their non-toxic property, tunabe optical behavior, gold nanomaterials are expected to integrate early diagnosis and therapy in one platform.[35,36] A variety of gold-based nanomaterials have been prepared as reagents for photothermal conversion.[37,38] However, according to the current situation, the design and construction of CYPA-targeted Au nanostar-based yolk-shell structure was not reported. It is necessary to fabricate the new nanostructure because it can develop a new method of tumor diagnosis and treatment to overcome the limitation of traditional tumor markers and traditional theranostic methods.

Inspired by these advantages, in this paper, we developed a novel CYPA-targeted SiO_2 encapsulated Au star@AgAu yolk-shell nanostructure (Au@AgAu YSNS), which could be used as "nano-theranostics" for ovarian cancer early diagnosis and therapy by SERS and PTT method, respectively. Au@AgAu YSNS were prepared by adjusting the Ag/Au ratios and its SERS performance was screened with Raman spectrometer. Then, SERS probe molecule crystal violet (CV) was absorbed on the surface of Au@AgAu YSNS, followed by SiO_2 encapsulation. Next, antibody was coupled with Au@AgAu@CV@SiO_2, which was employed to detect CYPA antigen proteins in plasma using the SERS method. In addition, the photothermal conversion performance Au@AgAu YSNS was also investigated. Experiments in vitro and in vivo were carried out, indicating that the prepared yolk-shell nanostructures could be employed as photothermal therapy agents for ovarian cancer.[39,40] The new information obtained from this study may be beneficial to promote the construction of novel nanostructures and their medical application.

Materials and Methods

Materials

The following are the chemical reagents necessary to complete this work, including chloroauric acid ($HAuCl_4 \cdot 4H_2O$), sodium citrate dihydrate ($C_6H_5Na_3O_7 \cdot 2H_2O$), hydrochloric acid (HCl), silver nitrate ($AgNO_3$), ascorbic acid (AA), cetyltrimethylammonium bromide (CTAB), N-hexadecyltrimethylammonium chloride (CATC), sodium hydroxide (NaOH), crystal violet (CV), 3-aminopropyltriethoxysilane (APTES), phosphate buffer saline (PBS), bovine serum albumin (BSA), human Cyclophilin A protein (CYPA), Human Cyclophilin A, Antibody CYPA. All chemicals square measure analytically pure and were used as received while not more purification. Deionized water was used throughout the experiment.

Preparation of SiO_2 Encapsulated Au@AgAu YSNS

The preparation of Au@AgAu YSNS was modified according to the related synthetic methods of nanorods.[25,41,42] Firstly, Au nanostar (Au NS) was synthesized according to the previous reports.[43] Then, to replace CTAB in AuNS solution, the prepared AuNS was first centrifugally washed with CTAC (80 mM) solution, and then 500 μL $AgNO_3$ (0.01M) and 25 μL ascorbic acid (0.1M) were added to the CTAC solution of AuNS. The solution was then placed in a water bath and reacted at 65°C for 4.5 h. After centrifugation and washing twice, Au@Ag core-shell nanostar (Au@Ag NS) solution was obtained. Then, 10 mL CTAB (0.1 M), 102.96 μL $HAuCl_4$ (24.28 mM), 100 μL AA (0.1 M), 10 μL NaOH (1M) were added into the as-prepared Au@Ag core-shell nanostar solution successively and incubated at 30°C for 12 h. After washing by centrifugation, Au nanostar@AgAu yolk-shell nanostructures were obtained.

SiO_2 Encapsulation and CYPA Antibody Modification

CV was added into the as-prepared Au@AgAu YSNS to form the CV- Au@AgAu YSNS, which showed obvious SERS signals. After washing by centrifugation and redispersion in 10 mL ethanol, 40 μL APTES (10%, w.t.) was added and stirred overnight. After washing by centrifugation and redispersion in 10 mL PBS solution, add CYPA antibody (100 μL, 10 μg/mL), incubate at 4°C for 24 hours, shake continuously during this period so that it does not precipitate, and then add bovine serum albumin (100 μL, w.t. 3%). Finally, the solution needs to be centrifuged and preserved at 4°C to maintain its effectiveness.

Enzyme-Linked Immunosorbent Assay (ELISA)

The level of anti-CYPA in Au@AgAu@CV@$SiO_2$was measured by ELISA according to the manufacturer's instructions (Shanghai Jining Shiye, China). The samples and standard substances were added into the micropores pre-coated with the

captured antigen of human CYPA. Biological antibodies were added for antibody biotinylation. After incubation and thorough, HRP labeled detection antibodies were added, and after incubation and thorough washing. With the substrate TMB color, TMB under the catalysis of peroxidase into blue, and under the action of acid into the yellow. The intensity of color was positively correlated with the level of human cyclophilin A antibody (CYPA Ab) in the sample. The absorbance (OD value) was measured at 450nm wavelength and the sample concentration was calculated.

Characterization

The morphology of as-prepared nanostructures was investigated on a transmission electron microscopy (TEM, FEI Tecnai 12, America). UV-vis absorption spectra were recorded on a UV-vis spectrometer (AOE, UV-1902, China). With the aid of Via Raman spectrometer (532 nm laser) and thermo scientific DXR3 smart Raman spectrometer (785 nm laser) at room temperature, the SERS performance were acquired on Renishaw in the vary of 600–1800 cm^{-1}.

Determination of CYPA with SERS

The prepared CYPA antibody modified Au@AgAu@CV@SiO_2 was added in CYPA protein with different concentrations in 2 mL glass bottle, followed by a constant temperature reaction at 37°C for 2 h, and then determined by DXR3 smart Raman spectrometer.

Photothermal Conversion Performance

In order to explore the photothermal conversion performance of Au@AgAu YSNS, we used 808 nm near infrared (NIR, Beijing Leibo Photoelectric Technology Co., Ltd.) laser thermal imager to characterize the nano preparation. The specific procedure was as follows: Au@AgAu YSNS suspension (1 mL) was added to an ordinary test tube, and 808 nm laser was placed to irradiate it. The temperature changes were recorded by an infrared thermal imaging camera throughout the whole process. The other photothermal experiments included different concentrations of dispersing solution of Au@AgAu YSNS, five "laser on–off" cycles. The conversion efficiency was also investigated using the same instrument.

The Anti-Cancer Performance of Au@AgAu YSNS in vitro

To evaluate the anticancer activity of CYPA targeted Au@AgAu@CV@SiO_2, normal ovarian cells IOSE80 and ovarian cancer A2780 cells were incubated with CYPA targeted Au@AgAu@CV@SiO_2 for cytotoxicity test and therapeutic effect. IOSE80 and A2780 lines were supplied by China Center for Type Culture Collection (Shanghai, China). The two kinds of cells were transplanted into 96-well plates containing DMEM medium (μL) for 24h. CYPA targeted Au@AgAu@CV@SiO_2 was added, and incubated for another 12 h. Then, add 10 μL CCK8 solution into each well, gently knock the culture plate to mix, and incubate in the incubator for 3h. Finally, OD values of each pore at 450nm wavelength were detected by enzyme marker, and the cytotoxicity results were obtained. A similar treatment was used to investigate cell death in cancer cells A2780 irradiated and unirradiated by near infrared laser (808 nm, 1.5 W/cm^2, 10 min). In order to more clearly reflect the effect of the prepared material on cell activity, cancer cells were first inoculated in 6-well plates, cultured with DMEM medium for 12h, and then treated with fresh DMEM medium containing CYPA targeted Au@AgAu@CV@SiO_2. After 12h incubation, the cells were irradiated by near infrared laser and treated by non-near infrared laser, and then the cells incubated with the material solution were stained with propidium iodide (PI), which could only stain DNA of dead cells, and calcein-AM, which could only stain living cells. After 10min, the distribution of living cells and dead cells was observed by fluorescence microscope.

The Anti-Cancer Performance of Au@AgAu YSNS in vivo

Male Balb/c mice (8 weeks, female) were used in our work. All experimental protocols involving animals were carried out with permission from the Institutional Animal Care and Use Committee (IACUC) of Xuzhou Medical University, and the procedures were as per the regulations and guidelines of IACUC (Guidelines for ethical review of experimental animal welfare in Xuzhou Medical University). A2780 cells ($1*10^7$ cells per mL in PBS) were subcutaneously injected into the right flanks of the mice to establish the tumor bearing mouse model. Three groups (n = 3 per group) were employed: (i) the control group mice were injected with saline; (ii) the mice were injected with nano (CYPA targeted

Au@AgAu@CV@SiO_2) of 6 mg/kg; (iii) the mice with laser irradiation (1.5/cm^2 W, 5min) and injection of nano (CYPA targeted Au@AgAu@CV@SiO_2) of 6 mg/kg. During the treatment, the size and weights of the tumors were monitored every two days for 2 weeks. Infrared thermography of the tumor was acquired in real time using a Fotric 225 infrared thermography camera, and the spatial temperature distribution was performed. Finally, we immediately took out the organs of mice for H&E staining to observe the damage degree of the nano-composite material to the organs.

Results and Discussion

Characterization of Au@AgAu YSNS

The morphology and of the as-prepared nanostructures were investigated by a transmission electron microscopy and UV-vis spectrum in Figure 1. Figure 1A depicts that uniform Au nanostars (Au NS) with about 70 nm in size were obtained according to the previous reports.[43] When $AgNO_3$ was introduced, a layer of silver on the surface of Au nanostars in Figure 1B, indicating the formation of Au star@Ag nanostructures (Au@Ag NS). After the addition of $HAuCl_4$, the outer silver shell of Au@Ag NS is eroded away by Au^{3+}, forming an approximately 80 nm yolk-shell nanostructure with Au nanostar inside and AuAg alloy layer on the outer surface in Figure 1C, which was named Au@AgAu YSNS. Au@AgAu YSNS has yolk-shell structure and many voids, which will enhance the SERS performance.[25,29] The UV-visible absorbance spectra further confirmed the formation of the Au@AgAu YSNS in Figure 1D. It can be observed that the absorption peak of Au nanostar is range from 600 to 900 nm, which agree with the early reports.[44] However, when the formation of Au@Ag nanostar, its absorption peak blue shifted to 475 nm, which is attributed to the formation of Ag layers on the surface of Au star. For Au@AgAu YSNS, the absorption peak further red shifted to about 650 nm due to the corrosion of Ag layer, which indicated

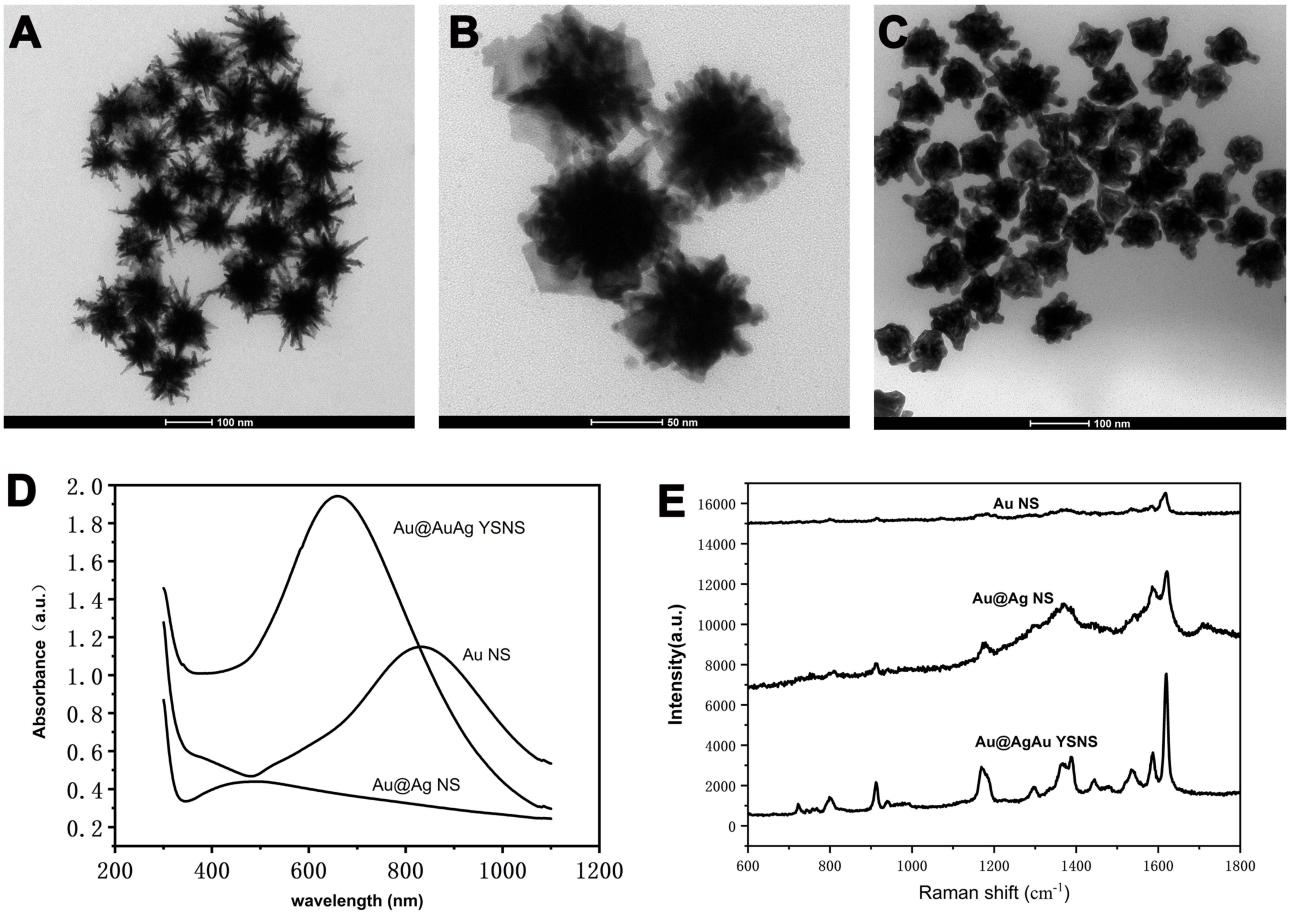

Figure 1 TEM images of (**A**) Au nanostar, (**B**) Au@Ag NS, (**C**) Au@AgAu YSNS (**D**) Ultraviolet spectra of Au nanostar, Au@Ag NS, Au@AgAu YSNS.(**E**) The SERS performance of Au NS, Au@Ag core-shell nanostructure and Au@Ag YSNS using CV (10^{-6} M) as probe molecule.

the successful preparation of Au@AgAu YSNS. Compared with other morphologies of noble metal nanostructures, the yolk-shell nanostructures with internal gaps were reported as ideal SERS substrates due to their high sensitivity. The SERS performance of Au stars, Au@Ag core-shell nanostructure and Au@Ag yolk-shell nanostructures were investigated by choosing crystal violet (CV) as Raman probes in Figure 1E. Typical Raman peaks of CV can be clearly determined. The intensity of SERS spectra of CV on Au@AgAu YSNS is 3.2 folds of that on Au@Ag core-shell nanostructure and 10.6 folds of that on Au nanostars. Herein, Au@AgAu YSNS were synthesized by replacement reaction using Au@Ag nanostars as sacrificial template and $HAuCl_4$ solution as etching agent, $HAuCl_4$ is essential to the formation of Au@AgAu YSNS. The impact of the ratio of $AgNO_3$ and $HAuCl_4$ on the formation of Au@AgAu YSNS and their SERS performance were also investigated in Figures S1 and S2. As the amount of chloroauric acid increased, the silver layer on the surface of Au NS was gradually eroded, and the star structure gradually diminished and egg yolk shell nanostars were formed. It can be found that many star like structures with branches were observed in 1:0.25 and 1:0.4 group, which indicated Au@AgAu YSNS has not been completely eroded away. However, little star like structures with branches were found in the 1:0.5 (Figure 1) 1:0.8, and 1:1 group (Figure S1). The Raman signal intensity gradually increases with the increase of the molar ratio of Ag: Au, reaching the maximum at 1:0.5, and then declines. It can be found that appropriate Ag/Au ratio plays a key role in the formation of Au@AgAu YSNS and their corresponding SERS performance.

Construction of CYPA Targeted, SiO_2 Encapsulated CV@Au@AgAu YSNS SERS Probe

Raman probe including tags molecules was widely used in biomedical detection and diagnostics. However, tag molecules often fall off during sample processing, resulting in inaccurate test. SiO_2 encapsulation is a good method to overcome this shortcoming.[45,46] To detect CYPA antigen proteins in plasma, CYPA antibody and SiO_2 encapsulated CV@Au@AgAu YSNS SERS probe was constructed in this work. Herein, CV, as a Raman tag molecule, was absorbed on the surface Au@AgAu YSNS due to its enhanced Raman signal. As shown in Figure 2A, obvious SERS signal was still found after encapsulation. TEM also confirmed that a thin layer of SiO_2 was found on the surface of CV@Au@AgAu YSNS in Figure S3. Furthermore, the surface of CV-Au@AgAu YSNS was hydroxylated or amino salinized by APTES process due to abundant active groups of APTES. The active groups on the surface of SiO_2 benefit the modification of CYPA-specific antibody. Thus, we fixed the CYPA-specific antibody to the surface of silica by reductive amination reaction with the amino group of the antibody. In order to show that CYPA-specific antibody was modified on the surface of nanomaterials, the antibody modified complex was characterized by ELISA, as shown in Figure S4. Au@AgAu@CV@SiO_2 and CYPA antibody modified Au@AgAu@CV@SiO_2 react with a standard substance of the same concentration to measure the antibody concentration on its surface. It can be seen that the nanomaterial coated with CYPA antibody reacts fully with the standard substance, and the attached antibody concentration can be obtained as 187.76 ng/mL in Figure S4. Due to the high specificity between antigen and antibody binding, the CYPA targeted, SiO_2 encapsulated CV@Au@AgAu YSNS SERS probe is capable of detecting CYPA at low concentrations.[47] For detection of CYPA, the SERS intensity depends seriously on volume ratio of antigen (0.01 μg/mL) to SERS probe in Figure 2B. And the good correlation exists between the concentration of CYPA antigen and SERS intensity within a certain range (10^{-7}μg/mL-10^{-2} μg/mL) in Figure 2C and D. To calculate the value of the limit of detection (LOD), we extended the standard curve in Figure 2D to its intersection point with the X-axis. The corresponding horizontal coordinate value is $7.76*10^{-10}$, which means the LOD value ($7.76*10^{-10}$ μg/mL). Obviously, the as-prepared Au@AgAu YSNS was feasible and highly sensitive for the determination of CYPA. Based on the above standard curve, this method was used to determine human serum diluted with known concentrations of PBS, and the results are shown in Table 1. It is obvious that this SERS method based on Au@AgAu YSNS are expected for early diagnosis of ovarian cancer.

Photothermal Conversion Performance of Au@AgAu YSNS

The strong absorption property of Au@AgAu YSNS in the near infrared region can make it play a unique advantage in the process of PPT cancer treatment. In order to better evaluate its photothermal properties, Au@AgAu YSNS was prepared into aqueous dispersions with gradient concentrations (20, 50, 100 and 200 μg/mL). They were irradiated with a laser of the same parameters (808 nm, continuous wave, 1 W/cm^2, 300 s) to collect their temperature changes. As shown in Figure 3A and B,

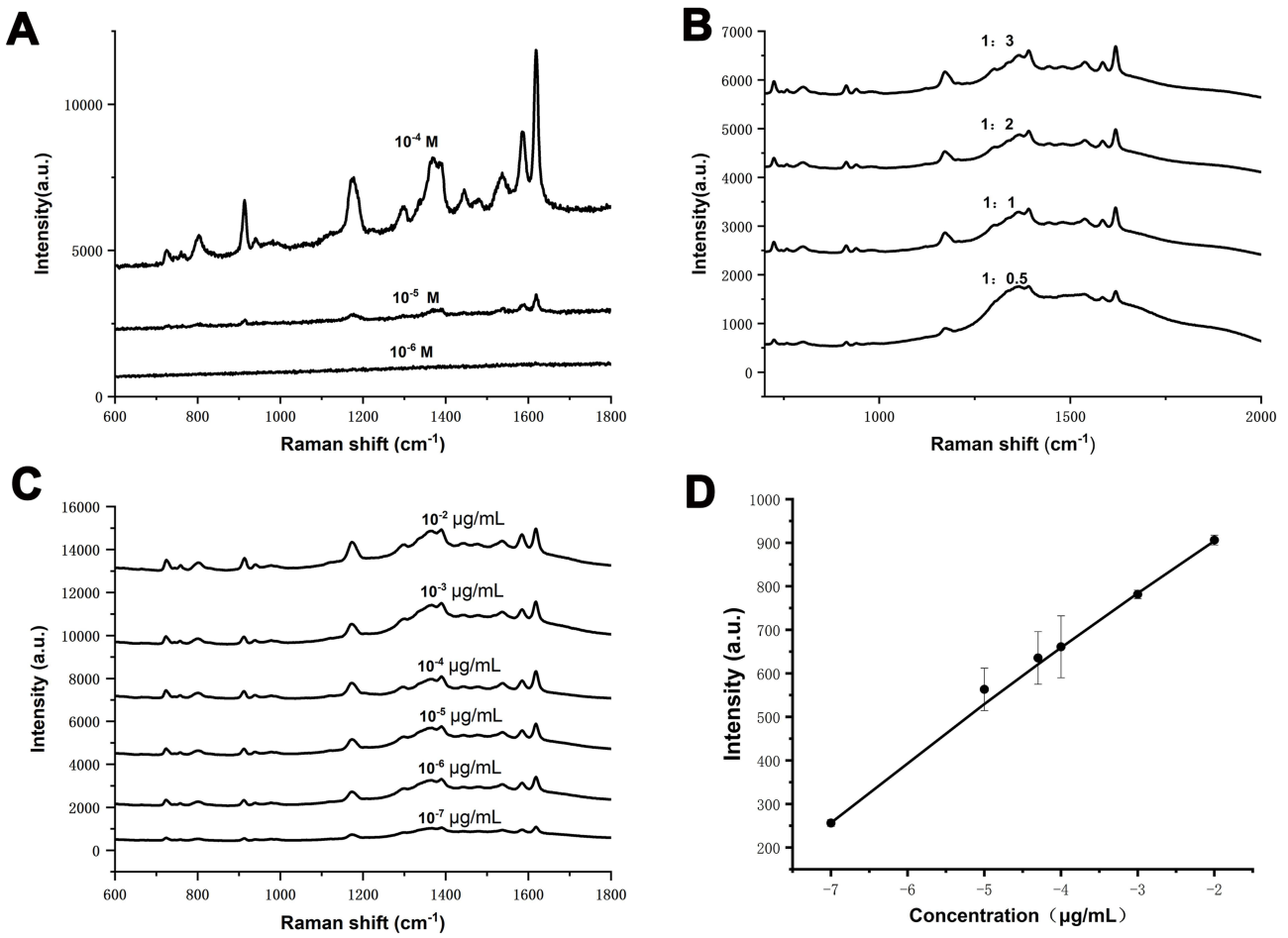

Figure 2 (**A**) The SERS spectra of Au@Ag@Au@CV@SiO_2 with different CV concentrations. (**B**) Raman spectra of Au@AgAu@CV@SiO_2 SERS probe (CV, 10^{-4} M) with different volume ratio of antigen (0.01 μg/mL, 100 μL) to Au@Ag@Au@CV@SiO_2 solution (400 μg/mL). (**C**) Raman spectra of different concentrations of CYPA. (**D**) Relationship between the negative logarithm of human serum CYPA concentration and peak height.

the increasing temperatures of Au@AgAu YSNS solutions are proportional to the concentration of the solutions. The temperature was increased to 58.7°C (35.7°C of the increasing temperatures) at a concentration of 200 μg/mL, which effectively proves that Au@AgAu YSNS has good photothermal performance. The photothermal stability was discussed in Figure 3C. Five cycles of laser on/off irradiation were performed. No significant temperature change during these cycles indicated good photostability of the as-prepared Au@AgAu YSNS. The photothermal conversion efficiency is also calculated in Figure 3D and E and the methods are shown in Supplementary Materials, which is about 38.72%. Obviously, the as-prepared Au@AgAu YSNS could be used as PTT agents for ovarian cancer.

The Anti-Cancer of Au@AgAu YSNS in vitro

As a PTT agent, high safety and in vitro cytocompatibility are essential. To verify whether the prepared CYPA targeted Au@AgAu@CV@SiO_2 (for the convenience of further discussion in vitro and in vivo experiment, CYPA targeted

Table 1 The Calculated CYPA Concentration in Human Serum Using SERS Methods

Sample	Actual Concentration (pg/mL)	Detection Concentrations (pg/mL)	RSD (%) n = 3
Human serum	20.23	22.62	25.07
	404.7	410.25	9.66

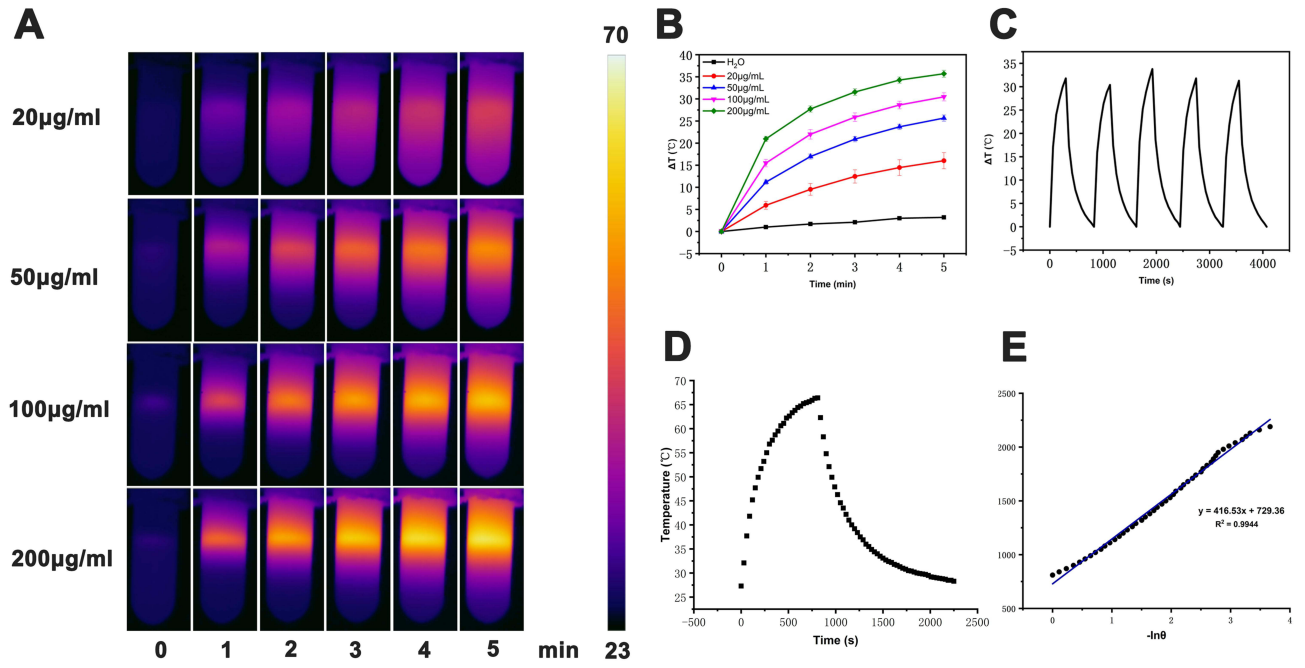

Figure 3 (**A**)Thermal infrared images of different concentrations of Au@AgAu YSNS (20, 50, 100, 200 μg/mL). (**B**) Heating curves of Au@AgAu YSNS at different concentrations (20,50,100,200 μg/mL) under an 808-nm laser irradiation (1 W cm^{-2}) with. (**C**) Temperature changes exhibited during five heating and cooling cycles (100μg /mL, 1 W cm^{-2}). (**D**) Heating-cooling curves of Au@AgAu YSNS (100μg /mL, 1 W cm^{-2}). (**E**) The linear relationship of time data versus −ln θ obtained from the cooling period of picture.

Au@AgAu@CV@SiO_2 was denoted "nano" in the following discussion) have the above two properties, normal ovarian cells were incubated with different concentrations of "nano" for 24 h. As shown in Figure 4A, the "nano" of each concentration had little damage to the cells. To discuss the anticancer of "nano" in vitro, ovarian cancer cells A2780 was co-incubated with

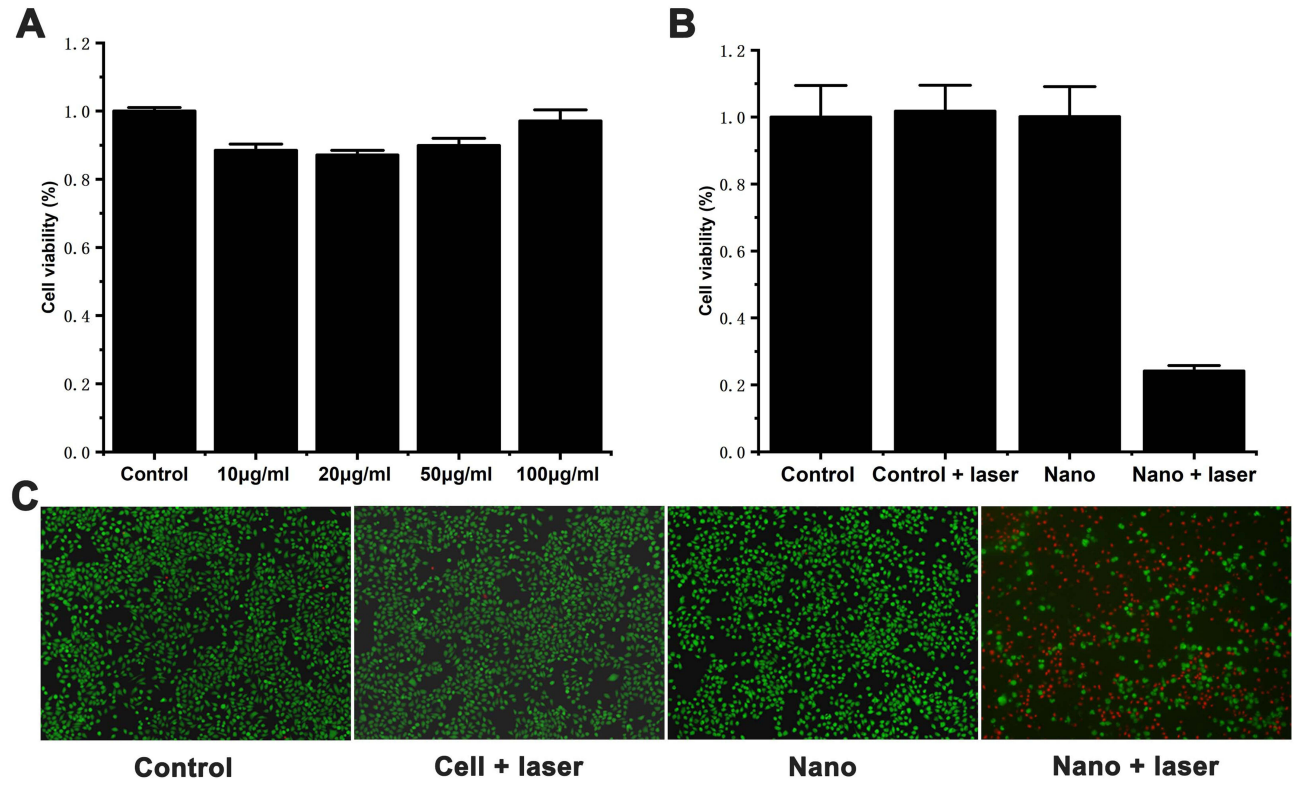

Figure 4 (**A**) Cell viability of normal ovarian cells incubated with different concentrations of nanomaterials for 24h. (**B**) Cell viability of A2780 ovarian cancer cells in different groups (the concentrations of nanomaterials is 50 μg/mL). (**C**) Calcein-AM and propidium iodide staining images of different groups A2780 ovarian cancer cells.

"nano". As can be seen Figure 4B, cell death rates were very low in the control (medium only), laser groups (laser only) and nano groups. However, both laser irradiation and "nano" were involved, the cell survival rate was only 24%, indicating that laser irradiation can activate "nano" to achieve PTT effect. To visually evaluate the anticancer properties, the cells stained with calcein-AM and propyl iodide were placed under fluorescence microscope to observe the survival of the cells. A small number of dead cells could be seen in the control (medium only), laser groups (laser only) and nano groups ("nano" only). However, as shown in Figure 4C, most of the cells died after being "nano"-treated under near-infrared irradiation. Apparently, the prepared CYPA targeted Au@AgAu@CV@SiO_2 was lethal to cancer cells.

The Anti-Cancer in vivo

The PTT efficacy of "nano" was further investigated in vivo in Figure 5. Real-time infrared thermal imaging photographs of saline and nano + laser treated tumor-bearing mice are shown in Figure 5A. It can be clearly concluded that the saline injection into the tumor was purple in the irradiation time, and there was no significant change (the temperature is 31.9°C). The tumors of mice in nano + laser group underwent a significant color change, from dark purple to bright pink, where the temperature has risen by about 10°C in just 5 min (the final temperature is 41.5°C). This will help kill tumor cells. In order to further explore its tumor efficacy, we observed the mice for 14 days, and then sacrificed the mice to remove the tumors. The volume and weight of tumor were investigated in Figure 5B–D. It can be inferred that the tumor volume can be significantly reduced in nano + laser group, completely different from the control group, indicating that "nano" has a high efficacy of PTT for cancer.

In order to explore whether "nano" has an unknown damaging effect on the internal body, H&E staining was used for in-depth exploration, and the experimental results are displayed in Figure 6. Principal organs such as heart, liver, spleen,

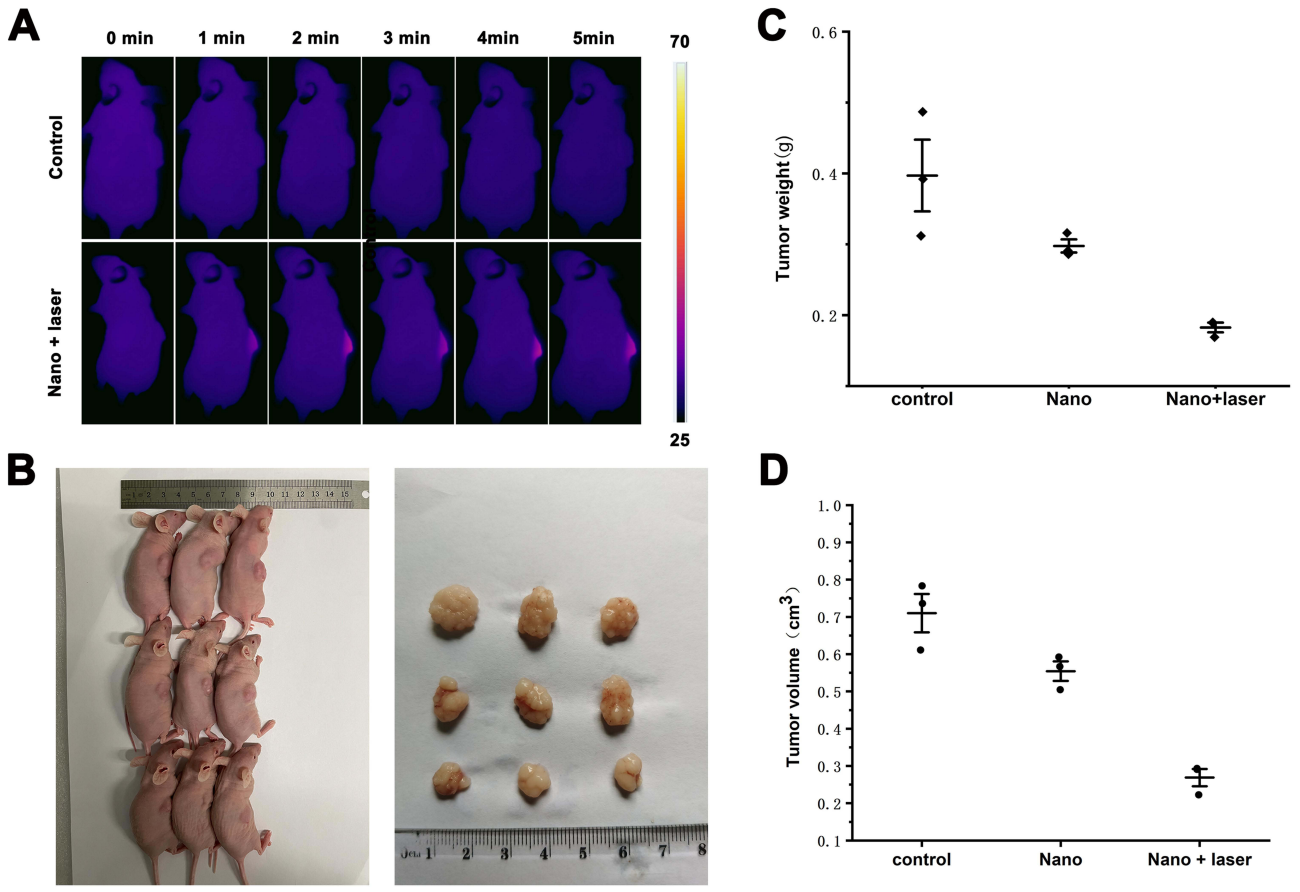

Figure 5 (**A**) Thermal infrared images of mice in control group and nano+laser (50 μg/mL, 808nm,1.5 W/cm^2, 5min). (**B**) Photographs of the tumors (n=3) that taken on the seventh day. (**C**) The curves of tumor weight (n = 3) for each experimental group. (**D**) The curves of tumor volume (n = 3) for each experimental group.

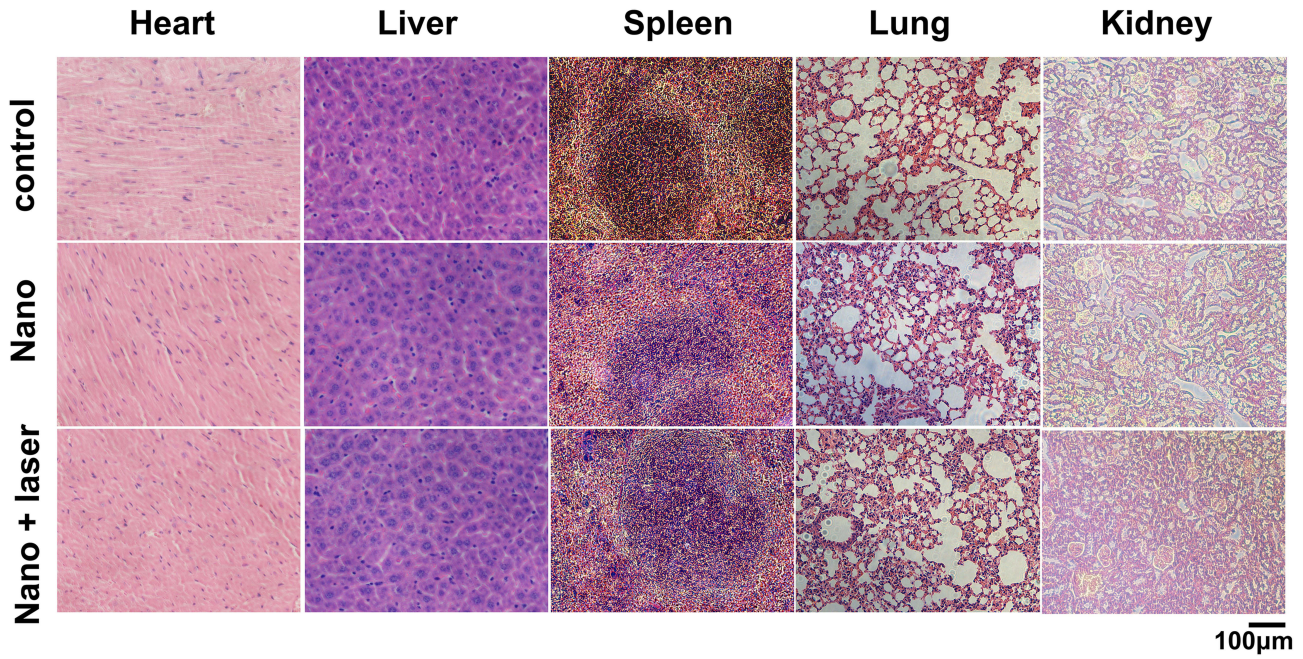

Figure 6 H&E staining after Au@AgAu@CV@SiO_2 injected into each organ of mice.

lung, and kidney were harvested for H&E staining. Compared with the nano group and the control group, the tissue necrosis in the "nano" group was not obvious. These results indicate that CYPA targeted Au@AgAu@CV@SiO_2 has a relatively low toxic effect on major organs of the body and has good histocompatibility, which can provide a new approach for the treatment of tumors in vivo.

Conclusion

In summary, we put forward a novel CYPA targeted bimetallic nano-theragnostic based on SERS for the detection of ovarian cancer marker and PTT for ovarian cancer. Experimental results showed that the ratio of silver nitrate ($AgNO_3$) to chloroauric acid ($HAuCl_4$) played a crucial part in the SERS performance. Employing this nano-theragnostic, low concentration of CYPA was measured in serum. In addition, the nano-theragnostic is also proven to have excellent photothermal conversion efficiency, which could be used as PTT for ovarian cancer. This work could provide a highly sensitive, rapid and simple diagnostic method for the detection of tumor biomarker CYPA. Meanwhile, it is also expected to realize the hope of photothermal treatment of cancer.

Acknowledgments

This work was financially supported by the Postdoctoral Research Funding Program of Jiangsu Province of China (1701133C), Science and Technology Innovation Project of Xuzhou City (KC22120) and Jiangsu Training Program of Innovation and Entrepreneurship for Undergraduates (202210313040Z).

Disclosure

The authors declare that they have no known competing financial interests or personal relationships that could have appeared to influence the work reported in this paper.

References

1. Siegel RL, Miller KD, Fuchs HE, Jemal A. Cancer statistics, 2022. *CA Cancer J Clin*. 2022;72(1):7–33. doi:10.3322/caac.21708
2. Moufarrij S, Dandapani M, Arthofer E, et al. Epigenetic therapy for ovarian cancer: promise and progress. *Clin Epigenetics*. 2019;11(1):7. doi:10.1186/s13148-018-0602-0

3. Labidi-Galy SI, Olivier T, Rodrigues M, et al. Location of mutation in BRCA2 gene and survival in patients with ovarian cancer. *Clin Cancer Res*. 2018;24(2):326–333. doi:10.1158/1078-0432.CCR-17-2136
4. Lowry KP, Lee SI. Imaging and screening of ovarian cancer. *Radiol Clin North Am*. 2017;55(6):1251–1259. doi:10.1016/j.rcl.2017.06.010
5. Chen Z, Liang Q, Zeng H, et al. Exosomal CA125 as a promising biomarker for ovarian cancer diagnosis. *J Cancer*. 2020;11(21):6445–6453. doi:10.7150/jca.48531
6. Funston G, Hamilton W, Abel G, Crosbie EJ, Rous B, Walter FM. The diagnostic performance of CA125 for the detection of ovarian and non-ovarian cancer in primary care: a population-based cohort study. *PLoS Med*. 2020;17(10):e1003295. doi:10.1371/journal.pmed.1003295
7. Qu W, Li J, Duan P, et al. Physiopathological factors affecting the diagnostic value of serum HE4-test for gynecologic malignancies. *Expert Rev Mol Diagn*. 2016;16(12):1271–1282. doi:10.1080/14737159.2016.1251317
8. Wang Q, Zhang M, Tomita T, et al. Selected reaction monitoring approach for validating peptide biomarkers. *Proc Natl Acad Sci U S A*. 2017;114(51):13519–13524. doi:10.1073/pnas.1712731114
9. Chu MY, Huang HC, Li EM, Xu LY. CypA: a potential target of tumor radiotherapy and/or chemotherapy. *Curr Med Chem*. 2021;28(19):3787–3802. doi:10.2174/0929867327666201029161055
10. Qi ZY, Wang F, Yue YY, et al. CYPA promotes the progression and metastasis of serous ovarian cancer (SOC) in vitro and in vivo. *J Ovarian Res*. 2019;12(1):118. doi:10.1186/s13048-019-0593-2
11. Forstner R. Early detection of ovarian cancer. *Eur Radiol*. 2020;30(10):5370–5373. doi:10.1007/s00330-020-06937-z
12. Pilyugin M, Ratajska M, Stukan M, Concin N, Zeillinger R, Irminger-Finger I. BARD1 autoantibody blood test for early detection of ovarian cancer. *Genes*. 2021;12(7):969. doi:10.3390/genes12070969
13. Liu T, Hou M, Li M, et al. Pyroptosis: a developing foreland of ovarian cancer treatment. *Front Oncol*. 2022;12:828303. doi:10.3389/fonc.2022.828303
14. Peng L, Jiang J, Chen HN, et al. Redox-sensitive cyclophilin A elicits chemoresistance through realigning cellular oxidative status in colorectal cancer. *Cell Rep*. 2021;37(9):110069. doi:10.1016/j.celrep.2021.110069
15. Krajczewski J, Kolataj K, Pietrasik S, Kudelski A. Silica-covered star-shaped Au-Ag nanoparticles as new electromagnetic nanoresonators for Raman characterisation of surfaces. *Spectrochim Acta A Mol Biomol Spectrosc*. 2018;193:1–7. doi:10.1016/j.saa.2017.11.060
16. Ren X, Li X. Flower-like Ag coated with molecularly imprinted polymers as a surface-enhanced Raman scattering substrate for the sensitive and selective detection of glibenclamide. *Anal Methods*. 2020;12(22):2858–2864. doi:10.1039/d0ay00575d
17. Pastorello M, Sigoli FA, Dos Santos DP, Mazali IO. On the use of Au@Ag core-shell nanorods for SERS detection of Thiram diluted solutions. *Spectrochim Acta A Mol Biomol Spectrosc*. 2020;231:118113. doi:10.1016/j.saa.2020.118113
18. Xu J, Cheng C, Shang S, Gao W, Zeng P, Jiang S. Flexible, reusable SERS substrate derived from ZIF-67 by adjusting LUMO and HOMO and its application in identification of bacteria. *ACS Appl Mater Interfaces*. 2020;12(44):49452–49463. doi:10.1021/acsami.0c15754
19. Dumont E, De Bleye C, Cailletaud J, et al. Development of a SERS strategy to overcome the nanoparticle stabilisation effect in serum-containing samples: application to the quantification of dopamine in the culture medium of PC-12 cells. *Talanta*. 2018;186:8–16. doi:10.1016/j.talanta.2018.04.038
20. Krajczewski J, Michalowska A, Kudelski A. Star-shaped plasmonic nanostructures: new, simply synthetized materials for Raman analysis of surfaces. *Spectrochim Acta A Mol Biomol Spectrosc*. 2020;225:117469. doi:10.1016/j.saa.2019.117469
21. Ramirez-Perez JC, Reis TA, Olivera CL, Rizzutto MA. Impact of silver nanoparticles size on SERS for detection and identification of filamentous fungi. *Spectrochim Acta A Mol Biomol Spectrosc*. 2022;272:120980. doi:10.1016/j.saa.2022.120980
22. Liu Y, Ma H, Han XX, Zhao B. Metal-semiconductor heterostructures for surface-enhanced Raman scattering: synergistic contribution of plasmons and charge transfer. *Mater Horiz*. 2021;8(2):370–382. doi:10.1039/d0mh01356k
23. Cui X, Li M, Tong L, Li M, Tang X, Han X. High aspect ratio plasmonic Au/Ag nanorods-mediated NIR-II photothermally enhanced nanozyme catalytic cancer therapy. *Colloids Surf B*. 2023;223:113168. doi:10.1016/j.colsurfb.2023.113168
24. Ma L, Chen Y-L, Yang D-J, et al. Gap-dependent plasmon coupling in Au/AgAu hybrids for improved SERS performance. *J Phys Chem C*. 2020;124(46):25473–25479. doi:10.1021/acs.jpcc.0c07701
25. Zhu J, Zhang S, Weng GJ, Li JJ, Zhao JW. The morphology regulation and plasmonic spectral properties of Au@AuAg yolk-shell nanorods with controlled interior gap. *Spectrochim Acta a Mol Biomol Spectrosc*. 2020;236:118343. doi:10.1016/j.saa.2020.118343
26. Vu TD, Duy PK, Chung H. Nickel foam–caged Ag-Au bimetallic nanostructure as a highly rugged and durable SERS substrate. *Sens Actuators B Chem*. 2019;282:535–540. doi:10.1016/j.snb.2018.11.098
27. Zhang F, Wu N, Zhu J, et al. Au@AuAg yolk-shell triangular nanoplates with controlled interior gap for the improved surface-enhanced Raman scattering of rhodamine 6G. *Sens Actuators B Chem*. 2018;271:174–182. doi:10.1016/j.snb.2018.05.095
28. Chen QQ, Hou RN, Zhu YZ, et al. Au@ZIF-8 core-shell nanoparticles as a SERS substrate for volatile organic compound gas detection. *Anal Chem*. 2021;93(19):7188–7195. doi:10.1021/acs.analchem.0c05432
29. Li Z, Yang F, Wu D, et al. Ce6-conjugated and polydopamine-coated gold nanostars with enhanced photoacoustic imaging and photothermal/photodynamic therapy to inhibit lung metastasis of breast cancer. *Nanoscale*. 2020;12(43):22173–22184. doi:10.1039/d0nr05386d
30. Gupta N, Malviya R. Understanding and advancement in gold nanoparticle targeted photothermal therapy of cancer. *Biochim Biophys Acta Rev Cancer*. 2021;1875(2):188532. doi:10.1016/j.bbcan.2021.188532
31. Ren Y, Yan Y, Qi H. Photothermal conversion and transfer in photothermal therapy: from macroscale to nanoscale. *Adv Colloid Interface Sci*. 2022;308:102753. doi:10.1016/j.cis.2022.102753
32. Ouyang R, Zhang Q, Cao P, et al. Efficient improvement in chemo/photothermal synergistic therapy against lung cancer using Bi@Au nano-acanthospheres. *Colloids Surf B*. 2023;222:113116. doi:10.1016/j.colsurfb.2022.113116
33. Huang X, Lu Y, Guo M, Du S, Han N. Recent strategies for nano-based PTT combined with immunotherapy: from a biomaterial point of view. *Theranostics*. 2021;11(15):7546–7569. doi:10.7150/thno.56482
34. Liu Y, Bhattarai P, Dai Z, Chen X. Photothermal therapy and photoacoustic imaging via nanotheranostics in fighting cancer. *Chem Soc Rev*. 2019;48(7):2053–2108. doi:10.1039/c8cs00618k
35. Mahmoudi A, Kesharwani P, Majeed M, Teng Y, Sahebkar A. Recent advances in nanogold as a promising nanocarrier for curcumin delivery. *Colloids Surf B*. 2022;215:112481. doi:10.1016/j.colsurfb.2022.112481

36. Huang J, Zhu Y, Liu C, et al. Fabricating a homogeneously alloyed AuAg shell on au nanorods to achieve strong, stable, and tunable surface plasmon resonances. *Small*. 2015;11(39):5214–5221. doi:10.1002/smll.201501220
37. Yuan H, Fales AM, Vo-Dinh T. TAT peptide-functionalized gold nanostars: enhanced intracellular delivery and efficient NIR photothermal therapy using ultralow irradiance. *J Am Chem Soc*. 2012;134(28):11358–11361. doi:10.1021/ja304180y
38. Xing T, Qian Q, Ye H, et al. Gold nanoparticles with helical surface structure transformed from chiral molecules for SERS-active substrates preparation. *Biosens Bioelectron*. 2022;212:114430. doi:10.1016/j.bios.2022.114430
39. Wang Z, Xu Z, Xu X, et al. Construction of core-in-shell Au@N-HCNs nanozymes for tumor therapy. *Colloids Surf B*. 2022;217:112671. doi:10.1016/j.colsurfb.2022.112671
40. Shang T, Yu X, Han S, Yang B. Nanomedicine-based tumor photothermal therapy synergized immunotherapy. *Biomater Sci*. 2020;8(19):5241–5259. doi:10.1039/d0bm01158d
41. Jiang R, Chen H, Shao L, Li Q, Wang J. Unraveling the evolution and nature of the plasmons in (Au core)-(Ag shell) nanorods. *Adv Mater*. 2012;24(35):OP200–OP207. doi:10.1002/adma.201201896
42. Priecel P, Adekunle Salami H, Padilla RH, Zhong Z, Lopez-Sanchez JA. Anisotropic gold nanoparticles: preparation and applications in catalysis. *Chin J Catal*. 2016;37(10):1619–1650. doi:10.1016/s1872-2067(16)62475-0
43. Yuan H, Khoury CG, Hwang H, Wilson CM, Grant GA, Vo-Dinh T. Gold nanostars: surfactant-free synthesis, 3D modelling, and two-photon photoluminescence imaging. *Nanotechnology*. 2012;23(7):075102. doi:10.1088/0957-4484/23/7/075102
44. Satapathy SS, Bhol P, Chakkarambath A, et al. Thermo-responsive PNIPAM-metal hybrids: an efficient nanocatalyst for the reduction of 4-nitrophenol. *Appl Surf Sci*. 2017;420:753–763. doi:10.1016/j.apsusc.2017.05.172
45. Wang X, Wang M, Jiang T, et al. Dual-functional Fe3O4@SiO2@Ag triple core-shell microparticles as an effective SERS platform for adipokines detection. *Colloids Surf A*. 2017;535:24–33. doi:10.1016/j.colsurfa.2017.09.025
46. Wen S, Miao X, Fan GC, et al. Aptamer-conjugated Au Nanocage/SiO2 core-shell bifunctional nanoprobes with high stability and biocompatibility for cellular SERS imaging and near-infrared photothermal therapy. *ACS Sens*. 2019;4(2):301–308. doi:10.1021/acssensors.8b00682
47. Quyen TTB, Chang CC, Su WN, et al. Self-focusing Au@SiO2 nanorods with rhodamine 6G as highly sensitive SERS substrate for carcinoembryonic antigen detection. *J Mater Chem B*. 2014;2(6):629–636. doi:10.1039/c3tb21278e